ACS Infectious Diseases

pubs.acs.org/journal/aidcbc

Article

Kinetic Characterization of SARS-CoV-2 nsp13 ATPase Activity and Discovery of Small-Molecule Inhibitors

Aliakbar Khalili Yazdi, Paknoosh Pakarian, Sumera Perveen, Taraneh Hajian, Vijayaratnam Santhakumar, Albina Bolotokova, Fengling Li, and Masoud Vedadi*

Cite This: *ACS Infect. Dis.* 2022, 8, 1533−1542

Read Online

ACCESS | Metrics & More | Article Recommendations | Supporting Information

ABSTRACT: SARS-CoV-2 non-structural protein 13 (nsp13) is a highly conserved helicase and RNA 5′-triphosphatase. It uses the energy derived from the hydrolysis of nucleoside triphosphates for directional movement along the nucleic acids and promotes the unwinding of double-stranded nucleic acids. Nsp13 is essential for replication and propagation of all human and non-human coronaviruses. Combined with its defined nucleotide binding site and druggability, nsp13 is one of the most promising candidates for the development of pan-coronavirus therapeutics. Here, we report the development and optimization of bioluminescence assays for kinetic characterization of nsp13 ATPase activity in the presence and absence of single-stranded DNA. Screening of a library of 5000 small molecules in the presence of single-stranded DNA resulted in the discovery of six nsp13 small-molecule inhibitors with IC_{50} values ranging from 6 ± 0.5 to 50 ± 6 μM. In addition to providing validated methods for high-throughput screening of nsp13 in drug discovery campaigns, the reproducible screening hits we present here could potentially be chemistry starting points toward the development of more potent and selective nsp13 inhibitors, enabling the discovery of antiviral therapeutics.

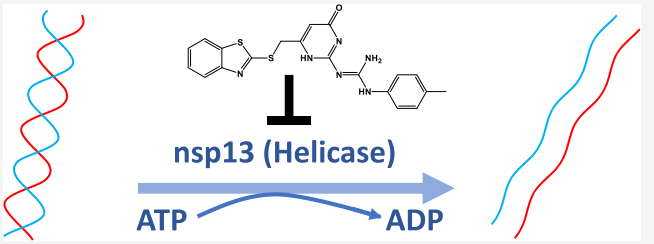

KEYWORDS: *SARS-CoV-2, COVID-19, helicase, ATPase, inhibitor, nsp13*

The COVID-19 pandemic, caused by SARS-CoV-2, has resulted in more than 6 million deaths to date and devastating global socioeconomic effects. Coronaviruses (CoVs) are major zoonotic viral pathogens, which belong to the Coronaviridae family, order Nidovirales.[1] Their genome is a large 26−32 kilobase single-stranded RNA, the largest known viral RNA genome,[2] which is responsible for production of 16 non-structural proteins (nsp1 to nsp16) and 4 structural and accessory proteins. Most non-structural proteins are involved in CoV replication and transcription through formation of the replication−transcription complex.[3] Among these proteins, nsp13 has been identified as a helicase capable of unwinding both DNA and RNA duplex substrates.[4−7] Along with the viral RNA-dependent RNA polymerase, nsp13 plays critical roles and is essential for CoV replication and propagation.[8−10]

Nsp13 is a member of superfamily 1 (SF1) helicases[6] and one of the most conserved proteins across Nidoviruses.[11] The crystal structures of coronaviral nsp13 also reveal a very high structural conservation.[12−14] It contains five domains, including an N-terminal zinc-binding domain, two RecA-like domains (1A and 2A), a stalk, and 1B domain. The zinc-binding domain, stalk, and 1B domains are believed to be involved in protein−protein or nucleic acid interactions within the replication−transcription complex.[8,10,15] The two RecA-like domains together form an active site for nucleoside triphosphate (NTP) binding and constitute a motor domain for nsp13, as its helicase function depends on its NTPase activity.[16,17] Like other known helicases, nsp13 RecA-like domains contain Walker motifs A and B, which carry highly conserved residues responsible for binding the terminal γ-phosphate group of NTP and coordination of Mg^{2+} ion of the NTP−Mg^{2+} complex.[18,19] In fact, the mutant of a conserved Lys residue within Walker B disrupted the unwinding activity of nsp13, which indicated that its helicase activity is dependent on the ATP hydrolysis.[13] RecA-like domains also carry the residues involved in binding their nucleic acid substrates.[14] Repeated conformational changes of the RecA-like motor domains through cycles of NTP binding and hydrolysis results in directional translocation of nsp13 along the nucleic acid substrate,[8,14,16] and it is believed that the unwinding activity of nsp13, similar to most helicases, is derived from its translocation on the single-stranded oligonucleotides.[14]

Nucleic acid stimulation of NTPase activity is a common characteristic of helicases.[4] Initial biochemical studies of coronaviral nsp13 have shown a basal ATPase activity, which

Received: March 25, 2022
Published: July 13, 2022

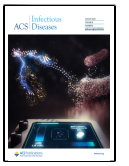

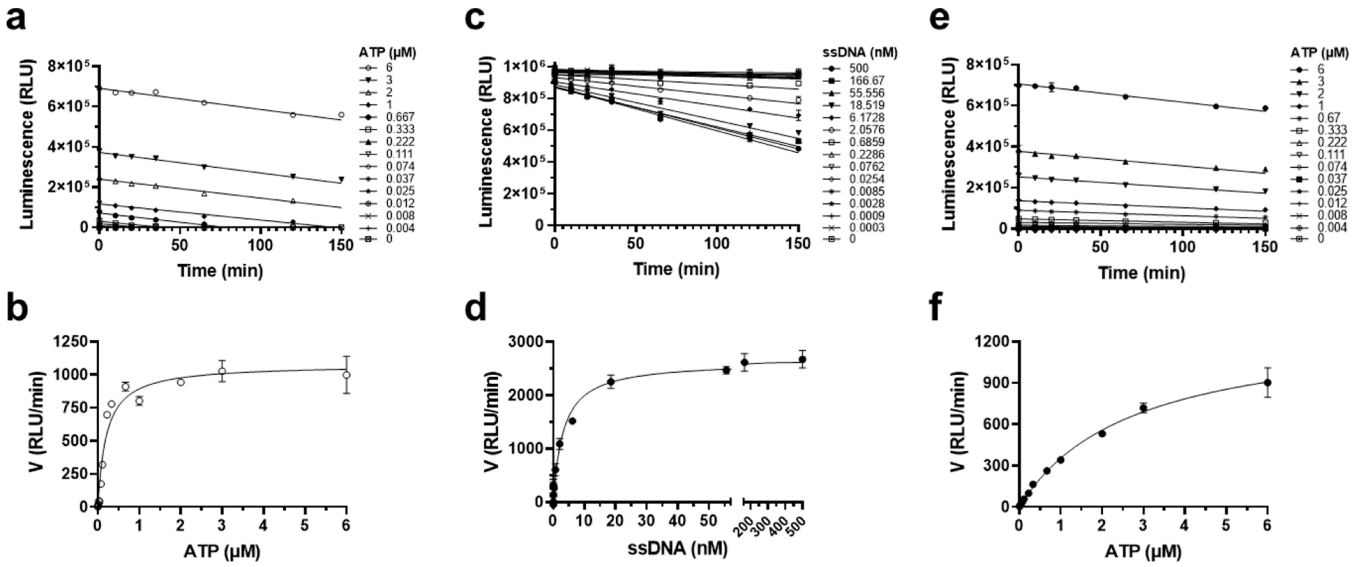

Figure 1. Kinetic characterization of nsp13 ATPase activity. (a,b) Kinetic characterization of ssDNA$^-$ ATPase activity: (a) initial velocities (ATP) and (b) K_m determination for ATP. (c–f) Kinetic analysis of ssDNA$^+$ ATPase activity: (c) initial velocities (ssDNA), (d) K_m determination for ssDNA, (e) initial velocities (ATP), and (f) K_m determination for ATP. The calculated kinetic parameters are presented in Table 1. Values in plots (a–f) are presented as the mean ± standard deviation of three independent experiments (n = 3). RLU: relative light unit.

is strongly stimulated by the presence of single-stranded (ss) nucleic acids (ssRNA and ssDNA).[4] Poly(dT), Poly(U), Poly(C), and Poly(dA) were most effective in stimulation of NTPase activity leading to an around 30- to 50-fold increase in activity.[4,7] Besides helicase activity, nsp13 also possesses a significant basal NTPase activity in the absence of any nucleic acids, that uses the same NTP binding site. However, ATP, dATP, and GTP are hydrolyzed most efficiently.[6] Likewise, nsp13 has an RNA 5′-triphosphatase activity through removal of the γ-phosphate group of the 5′- terminal nucleotide of RNA substrates using the same NTPase active site.[5,6] Because the cleavage of the phosphodiester bond between the β- and γ-phosphate groups of 5′-terminal nucleotide of RNA is the first step in 5′ mRNA capping, it is suggested that nsp13 may play a role in the coronaviral 5′ mRNA cap formation.[5] This is essential for evading the human immune system and virus propagation.[20]

Nsp13 is one of the most important targets for development of antiviral therapeutics for CoVs due to its high conservation among CoVs.[10,12,14,21,22] Structural studies have also identified druggable pockets on nsp13 protein which are highly conserved within the SARS-CoV-2 proteome.[12] Potent and selective inhibitors of nsp13 thus could provide a broad-spectrum antiviral effect. Here, we report on the development of parallel bioluminescence ATPase assays for characterization and screening potential inhibitors against (1) the basal NTPase activity of nsp13 (here on called ssDNA$^-$ ATPase), and (2) the ssDNA-stimulated NTPase activity (here on called ssDNA$^+$ ATPase). We employed the ssDNA$^+$ ATPase assay for screening and identifying small-molecule inhibitors of nsp13 that could be further developed toward potent inhibitors and viral therapeutics.

RESULTS AND DISCUSSION

SARS-CoV-2 nsp13 is a helicase and RNA 5′-triphosphatase.[6] Nsp13 exhibits NTPase activity with a diverse set of substrates, hydrolyzing ATP, dATP, and GTP.[6] The nsp13 ATPase activity which is required for helicase function is further stimulated (20–50 fold) in the presence of single- stranded polynucleotides (ssRNA and ssDNA).[4] The ssRNA [Poly(U) and Poly(A)] and ssDNA [Poly(dT) and Poly(dA)] show the same level of ATPase activation of nsp13 from various CoVs.[4,7,23,24] We took advantage of the existing Kinase-Glo reagents to monitor the change of ATP concentration in solution (Supporting Information Figure S1), for kinetic characterization of nsp13 ssDNA$^-$ and ssDNA$^+$ ATPase activities. The generated bioluminescent signal directly correlates with the amount of remaining ATP in the reaction and inversely with the level of ATPase activity of nsp13. Our initial tests using ATP as a substrate and a 30b PolyT ssDNA indicated that our recombinantly purified SARS-CoV-2 nsp13 (Supporting Information Figure S2) is highly active (data not shown). Therefore, we optimized and used this assay for kinetic characterization of nsp13 ATPase activities.

Assay Optimization. To facilitate the subsequent enzyme kinetic studies, we assessed the nsp13 ATPase activity through enzyme titration and proceeded with testing a series of buffers and additives to select the optimum conditions that generated the highest signal-to-noise ratio for nsp13 ssDNA$^-$ and ssDNA$^+$ ATPase activities. It has already been established that the presence of the DNA enhances the NTPase activity of nsp13.[4,7] We chose to perform all nsp13 ATPase assay optimizations in ssDNA$^+$ and ssDNA$^-$ (Supporting Information Figure S3). To better evaluate the effect of ssDNA on nsp13 ATPase activity, we needed to quantify and subtract the basal ATPase activity (ssDNA$^-$). Therefore, it was critical to choose a condition that maintained a significant window between the signals from these two activities (±ssDNA). We tested the effect of salts (NaCl, KCl), detergent (Triton X-100), reducing agent (DTT), bovine serum albumin (BSA), and DMSO through titration of each reagent in both assays (Supporting Information Figure S3). Low concentrations of KCl and NaCl (up to ∼30 mM) increased the ATPase activity in ssDNA$^-$ by about 2-fold. However, in ssDNA$^+$, salt had a significant negative effect on ATPase activity even at concentrations as low as 15 mM. Addition of 0.01% BSA led

https://doi.org/10.1021/acsinfecdis.2c00165
ACS Infect. Dis. 2022, 8, 1533–1542

Table 1. Kinetic Parameters for nsp13 ssDNA$^-$ and ssDNA$^+$ ATPase Activities[a]

enzyme	activity	substrate	K_m^{app} (nM)	k_{cat}^{app} (min^{-1})	$k_{cat}/K_{m,ATP}^{app}$ (min^{-1} nM^{-1})
nsp13	ssDNA$^-$ ATPase	ATP	210 ± 20	20 ± 1	0.095 ± 0.003
nsp13	ssDNA$^+$ ATPase	ATP	2800 ± 1000	300 ± 70	0.107 ± 0.015
		ssDNA	3.2 ± 0.2	580 ± 20	

[a]All experiments were performed in triplicate, and data are shown as the mean ± standard deviation.

to a parallel increase in ATPase activities in both ssDNA$^-$ and ssDNA$^+$ conditions. The presence of Triton X-100 led to a dramatic increase (2−5-fold) in ATPase activity under both conditions. Addition of DTT had a minimal effect with the highest signal for both reactions at 3 mM. DMSO, which is commonly used in preparation and screening of compounds, had little effect on nsp13 ATPase activity under both conditions up to 5%. Taken together, based on these results, two buffer combinations were chosen for additional assay optimization experiments (Supporting Information Figure S3g,h): buffer A (50 mM HEPES pH = 7.5, 20 mM NaCl, 5% glycerol, 5 mM magnesium acetate, 3 mM DTT, 0.01% BSA, and 0.01% Triton-X100) and buffer B (50 mM HEPES, pH = 7.5, 5% glycerol, 5 mM magnesium acetate, 5 mM DTT, and 0.01% BSA). Accordingly, through nsp13 titration tests in these buffers and by assessing the linear range of the response curve, it was clear that nsp13 was significantly more active in buffer A. However, the signal window for discriminating between the basal ATPase activity and the ATPase activity derived from stimulation by ssDNA significantly decreased under this condition. Buffer B, on the other hand, resulted in a higher level of ATPase activity in ssDNA$^+$ and a better signal window between the nsp13 activity in the presence and absence of ssDNA. At concentrations between 50 and 150 pM of nsp13, the positive effect of ssDNA on ATPase activity was more pronounced. Therefore, the results obtained through assay optimization experiments led to the selection of buffer B as the optimal buffer, which overall is the same as the buffers used in the previous nsp13 studies,[5,19,24,25] except for removing NaCl and increasing DTT to 5 mM. This optimized condition was used for all the subsequent kinetic and inhibition studies as described in Methods.

Kinetic Parameters of SARS-CoV-2 nsp13 ssDNA$^-$ ATPase Activity. The kinetic parameters for the ATPase activity of nsp13 under ssDNA$^-$ were determined in a 384-well format by assessing the initial velocities at various concentrations of ATP as the substrate (0.004−6 μM) and 0.5 nM of nsp13 using the selected buffer condition (Figure 1a,b). Under these conditions, 500 pM of nsp13 provided a measurable signal in all experiments while the initial velocities for ATPase activity were linear. The slopes of the linear initial velocity of reactions were determined and were used to calculate kinetic parameters. In ssDNA$^-$, a K_m^{app} of 210 ± 20 nM for ATP with a k_{cat}^{app} of 20 ± 1 min^{-1} was determined (Figure 1b). The obtained K_m^{app} for ATP is comparable to the previously reported values for SARS-CoV nsp13 (1.23 ± 0.12 μM).[6]

Kinetic Parameters for the nsp13 ssDNA$^+$ATPase Activity. Nsp13 helicase activity was assessed by measuring its polynucleotide-stimulated ATPase activity using ssDNA (30b PolyT) and ATP as substrates. It had been shown that both ssRNA and ssDNA could stimulate helicase activity in vitro.[4] PolyT (along with Poly U, A, and dA) have been shown to have the highest level of NTPase activation.[4,7] Using the optimized luminescence assay, the linear initial velocities of nsp13 in the presence of ssDNA (Figure 1c,e) were used to calculate the kinetic parameters (Figure 1d,f). Because in the presence of the polynucleotide the NTPase activity is significantly stimulated, lower concentrations of the nsp13 enzyme were used to maintain the linearity of the reaction within this set of experiments. Therefore, only 0.04 nM of nsp13 was used for determining the kinetic parameters for ssDNA$^+$ ATPase activity. After the initial estimation of kinetic values, for determination of the K_m of ssDNA, the ATP concentration was kept at 8.5 μM (~3× K_m of ATP), whereas the concentration of ssDNA was varied (0.0003−500 nM) (Figure 1c,d). A K_m^{app} of 3.2 ± 0.2 nM was obtained for ssDNA with a k_{cat}^{app} value of 580 ± 20 min^{-1} (Figure 1d and Table 1). For calculating the K_m of ATP, the linearity of initial velocities was measured at various concentrations of ATP (0.004−6 μM), whereas the concentration of the ssDNA was kept constant at 12 nM (Figure 1e,f). A K_m^{app} of 2800 ± 1000 nM was obtained for ATP for ssDNA$^+$ with a k_{cat}^{app} of 300 ± 70 min^{-1} (Figure 1f and Table 1). The variation in k_{cat}^{app} values (300 ± 70 and 580 ± 20; Table 1), obtained from K_m determination experiments for ATP and ssDNA, could be due to less than fully saturated concentrations of the second substrate. Compared to the ssDNA$^-$, the presence of ssDNA led to around 10-fold increase in the K_m^{app} of ATP (Table 1), consistent with the previous report for 299E-CoV nsp13 ATPase activity.[5] At the same time, clearly the presence of ssDNA stimulated the ATPase activity of nsp13 by more than 20-fold (Table 1). Therefore, the catalytic efficiency of nsp13 for ATP ($k_{cat}/K_{m,ATP}^{app}$) remained roughly the same for ssDNA$^+$ and ssDNA$^-$ ATPase activities (Table 1). One can speculate that with the same catalytic efficiency, low K_m of ATP and slow turnover (low k_{cat}) could facilitate binding to the RNA, followed by fast turnover needed for the helicase activity in cells. This is consistent with observations that ATP binding is promoting helicase DNA engagement.[26] The observed increase in the apparent turnover of nsp13 ATPase activity in the presence of ssDNA is in agreement with the reported observations.[4,7]

Amenability of Assays to High-Throughput Screening. High-throughput screening campaigns are typically carried out under balanced conditions (K_m of the substrates). This is an ideal screening condition that allows the small-molecule inhibitors to compete with substrates and be detected. Because the luciferase-based bioluminescence assay used for detecting the remaining ATP in this study is an endpoint assay, it was equally important to ensure that the signal-to-noise ratio at such conditions are reliable for screening and also the initial velocities are linear for the duration of the assay for better hit detection and accurate IC_{50} determination in the follow-up experiments.

Thus, the level of the obtained signal-to-noise ratio as well as the linearity of the initial velocities were further assessed in the selected screening conditions. Examining the activity of nsp13 at 0.1 nM enzyme and 0.25 μM ATP revealed that ssDNA$^-$ ATPase reaction can maintain its linearity for 1 h and an excellent signal-to-noise ratio was attained (Figure 2a). The

https://doi.org/10.1021/acsinfecdis.2c00165
ACS Infect. Dis. 2022, 8, 1533−1542

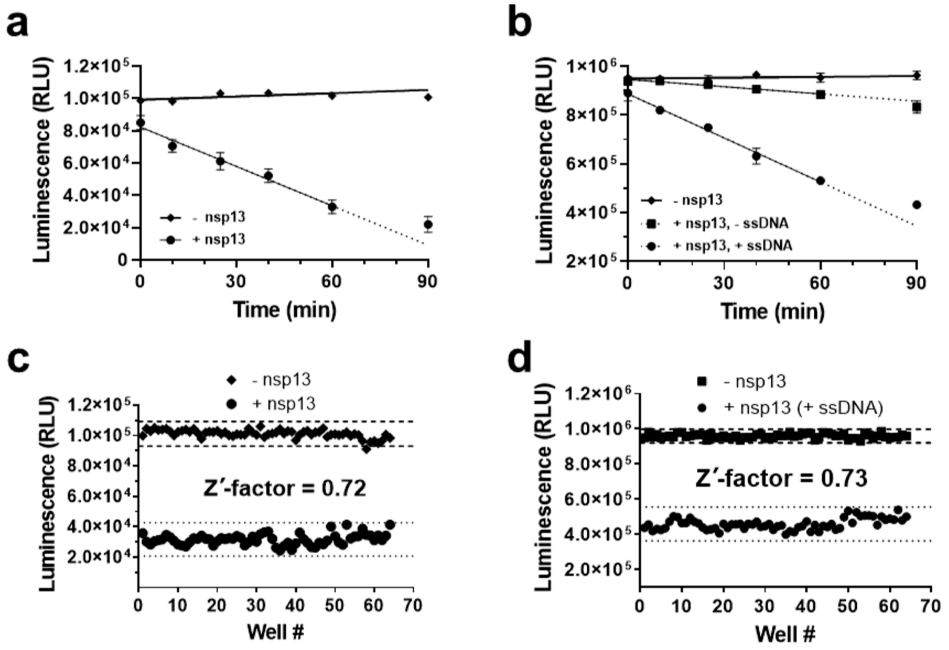

Figure 2. Amenability of the assays for high-throughput screening. (a) Linearity of ATPase activity of nsp13 was tested at K_m of ATP (0.25 μM ATP), ssDNA$^-$, and (b) at K_m for both ATP and ssDNA (ssDNA$^+$). Both ssDNA$^+$ ATPase activity (●: 2.5 μM ATP and 3.5 nM ssDNA) and the ssDNA$^-$ ATPase activity (■: only 2.5 μM ATP) performed under the same conditions are shown. The slight upward drift in the signal in the absence of nsp13 in "a" is due to variation of data points. Experiments in plots a and b were performed in quadruplicate. (c) Z'-factor of 0.72 was obtained for nsp13 ATPase assay under the screening conditions in a 384-well format in the (●) presence and (⧫) absence of nsp13. (d) ssDNA$^+$ assay was also amenable to screening in a 384-well format with a Z'-factor of 0.73. The dashed and dotted lines in panels c and d represent three standard deviations from the mean of each control group.

ssDNA$^+$ activity of nsp13 at 2.5 μM ATP, and 3.5 nM ssDNA (ssDNA$^+$), and 0.1 nM enzyme was linear for 1 h as well (Figure 2b).

Subsequently, the reproducibility and robustness of the assays for the high-throughput analysis were assessed. The nsp13 ATPase assays in a 384-well screening format had Z'-factors of 0.72 (Figure 2c) and 0.73 (Figure 2d) for ssDNA$^-$ and ssDNA$^+$, respectively. Assays with Z'-factors above 0.5 are typically considered reliable for high-throughput screening.[27,28]

It is important to note that similar to other endpoint assays, any changes to substrate concentration in the assay (in this case ATP) necessitates the fine-tuning of the reaction with respect to the enzyme concentration and incubation time to ensure that the signal-to-noise ratio is reliable and linearity of the assay is retained. Examples of such cases are when the screening needs to be performed at higher or lower concentrations than K_m of ATP and when assessing the potential ATP competitive pattern of inhibition of identified inhibitors by measurement of IC_{50} values at various concentrations of the ATP substrate.

Screening SARS-CoV-2 nsp13 against a 5K Library of Small Molecules. As ATP is essential for nsp13 activities, we targeted the nucleotide binding site. We employed the optimized ssDNA$^+$ ATPase assay for screening nsp13 against a library of 5000 small molecules at 50 μM. Seventeen compounds showed a higher than 50% inhibitory effect (Figure 3).

Out of these 17 compounds, 11 were commercially available, and their inhibitory effect was re-tested. Eight hits were reproducible and inhibited the ssDNA$^+$ ATPase activity of nsp13 with IC_{50} values ranging from 6 ± 0.5 to 330 ± 30 μM (Figure 4 and Table 2). The inhibitory effects of these compounds on the ssDNA$^-$ ATPase activity of nsp13 were also

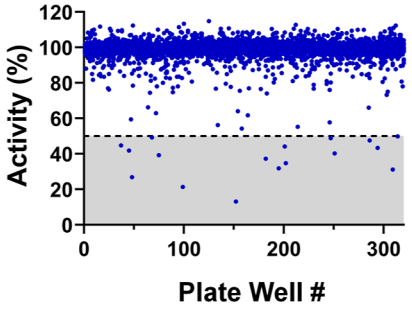

Figure 3. Screening nsp13 against a library of 5000 small molecules. SARS-CoV-2 nsp13 was screened against a library of 5000 potential kinase inhibitors at 50 μM on 16 384-well plates (n = 1). Compounds showing above 50% inhibition are highlighted in the gray area.

assessed. Only five compounds inhibited the ssDNA$^-$ ATPase activity as well with IC_{50} values ranging from 33 ± 2 to 240 ± 40 μM (Figure 4 and Table 2). For both ssDNA$^-$ and ssDNA$^+$ activities, assay data were normalized and samples in the presence and absence of the enzyme were used as controls for the 100 and 0% activities, respectively. Importantly, samples lacking the ssDNA but containing 2.5 μM ATP (same as the ATP concentration in the ssDNA$^+$ condition) were tested and the basal ATPase activity of ssDNA$^+$ experiments was measured. It was revealed that around 20−25% of the ATPase activity in the ssDNA$^+$ condition was rooted from the ssDNA independent ATPase activity of nsp13. This basal activity is also plotted in Figure 2b (■) for the condition that nsp13 is present but no ssDNA was added. This level of basal ATPase activity was not unexpected because the concentration of ATP in ssDNA$^+$ condition is around 10-fold of the K_m^{app} of ATP for the nsp13 ssDNA$^-$ activity. Notably, compounds C1 and C2

https://doi.org/10.1021/acsinfecdis.2c00165
ACS Infect. Dis. 2022, 8, 1533−1542

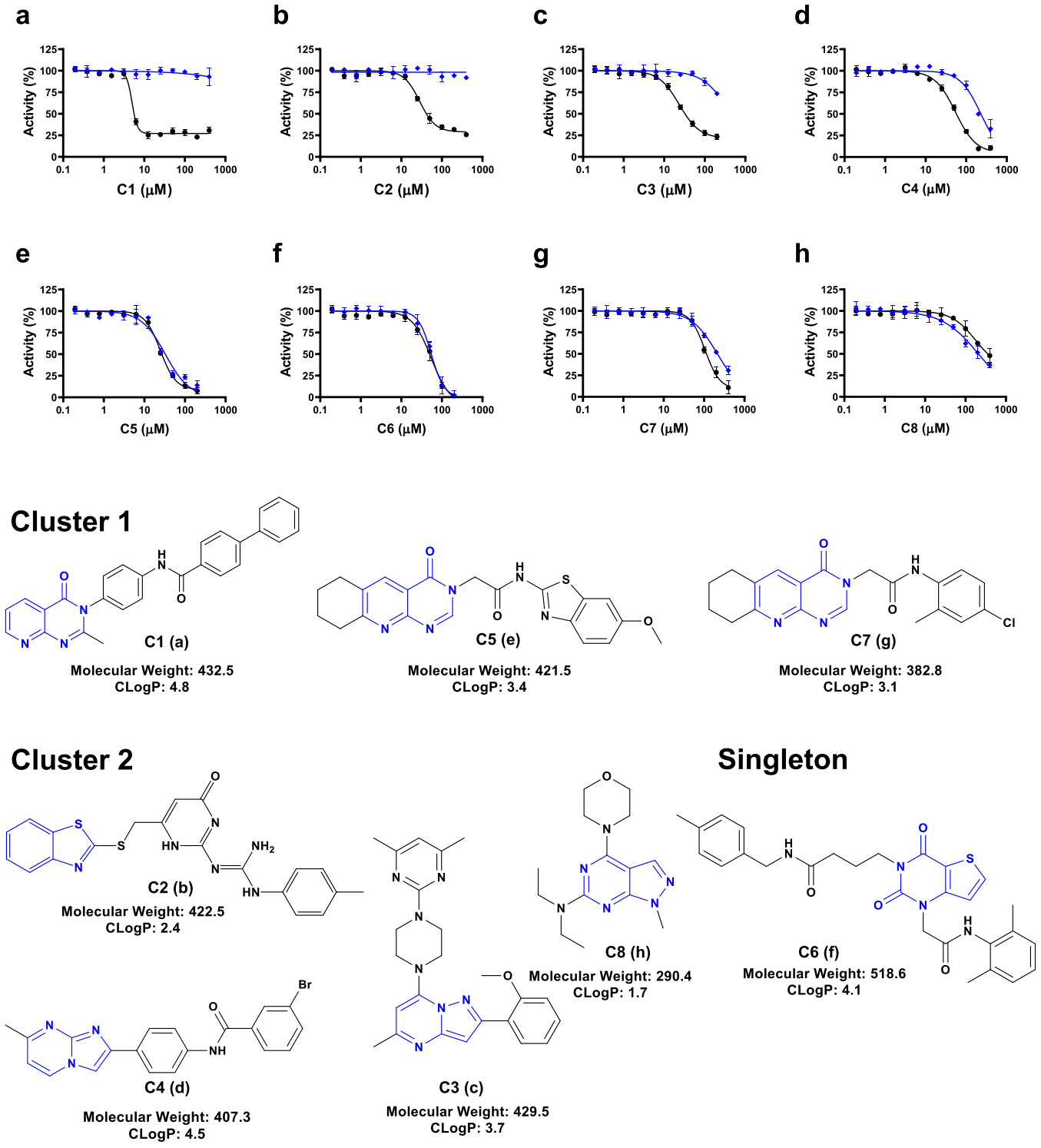

Figure 4. Inhibition of ATPase activity by reproducible hits. IC_{50} values were determined for the eight reproducible hits from the screening campaign (a–h). The experiments were performed in ssDNA$^+$ (black: ●) and ssDNA$^-$ (blue: ●) with compound concentrations of 195 nM to 400 μM. All experiments were performed using the optimized assay and values in (a–h) represent the mean ± standard deviation of three independent experiments (n = 3). Assay data are normalized to 0 and 100% nsp13 activity, and data in ssDNA$^+$ (black: ●) are presented without subtracting the basal ssDNA$^-$ ATPase activity. IC_{50} curves were generated using GraphPad Prism 9 using the four-parameter logistic equation and variable Hill slope. Chemical structures are presented in the bottom panel. The letters in parentheses under each structure indicate the corresponding IC_{50} curve.

(Figure 4) only inhibited nsp13 ssDNA$^+$, but not the ssDNA$^-$ ATPase activity. For these two compounds, the nsp13 inhibition reached a plateau. Regardless of the compound concentrations used, they did not reduce the activity of nsp13 by more than 75%. Combined with the absence of any ssDNA$^-$ ATPase inhibitory effects, it is possible that these compounds solely inhibited the ssDNA stimulation of nsp13 activity. The remaining 25% of nsp13 activity observed in the

https://doi.org/10.1021/acsinfecdis.2c00165
ACS Infect. Dis. 2022, 8, 1533−1542

Table 2. IC_{50} Determination for Eight Reproducible Inhibitors of nsp13 $ssDNA^+$ ATPase Activity[a]

compound	$ssDNA^+$ ATPase (μM)	Hill slope	$ssDNA^-$ ATPase (μM)	Hill slope
C1	6 ± 0.5	6[b]	NI	NA
C2	42 ± 3	2.3	NI	NA
C3	32 ± 2	1.7	>400	1.3
C4	57 ± 3	1.7	240 ± 40	1.7
C5	27 ± 1	2.3	33 ± 2	1.5
C6	50 ± 6	1.9	55 ± 3	2.7
C7	115 ± 10	2.4	215 ± 20	1.4
C8	330 ± 30	1.5	210 ± 20	1.0

[a]Values are from Figure 4. NI: no inhibition. [b]High Hill slope may indicate compound solubility limit.[30,31]

presence of these compounds is expected to arise from its basal ssDNA independent ATPase activity. The estimated Hill slopes for these compounds were steeper (6.0−2.3). A steep Hill slope could be explained by possible compound solubility issues at high concentrations, or other mechanisms such as cooperative unfolding or aggregation of the protein in the presence of a particular compound, or possibly binding of several inhibitor molecules to nsp13, possibly at the RNA binding site.[29,30] However, because these compounds do not interrupt the activity of nsp13 in the $ssDNA^-$ condition, these observations may be an indicative of a more complex (likely mixed) mode of binding for these compounds to nsp13 in the presence of ssDNA. On the other hand, compounds C5 and C6 inhibited $ssDNA^+$ and $ssDNA^-$ ATPase activities of nsp13 with relatively low and similar IC_{50} values (Figure 4e and Table 2).

As a counter screen, we optimized an assay for an unrelated protein, an aminoacyl-tRNA synthetase with ATPase activity using the same luciferase assay. Interestingly, none of the eight compounds showed any inhibitory effect in the counter screening (Supporting Information Figure S4). The results confirmed that these eight compounds do not interfere with the assay readout and are not nonspecific binders.

All eight hits (Figure 4) are druglike molecules with molecular weights of less than 450 Da, except for C6 (518.6 Da). Their CLogP are less than 4 except for C1 (4.8), C4 (4.5), and C6 (4.1), and they have no undesired functional groups. These compounds have some similarities and can be clustered into two main clusters and a singleton: cluster 1 includes C1, C5, and C7 which have pyridopyrimidine-4-one core structure (highlighted in blue), and cluster 2 includes C2, C3, C4, and C8 which have similar 6−5 ring systems (highlighted in blue). A singleton, C6 also has a 6,5 ring system but has thienopyrimidine-2,4-dione core as well as arylacetamide substitution similar to cluster 1, which indicates that some of the SAR features could be translated from one cluster to the other. Both clusters can be readily synthesized from commercially available building blocks. SAR of the cluster 1 can be explored by simple alkylation and amide coupling and by cross-coupling reactions. Similarly, SAR of the cluster 2 can also be readily explored by simple SNAr reactions with various amines and by cross-coupling reactions. As the hits were obtained from a kinase library, some of these hit compounds may also have kinase activity which needs to be monitored during the hit to lead campaign. C6 does not have the usual kinase hinge binding motif, which shows that the nsp13 inhibition can be maintained without the kinase binding motif present and therefore the kinase hinge binding motif of both clusters also could be removed without losing the nsp13 inhibitory effect.

Although we were unable to source 6 out of 17 compounds to confirm from powder, we proceeded with re-testing their inhibitory effects by using the original in-house compound samples. As such, we have provided the chemical structures of these compounds along with IC_{50} values and counter screen data to avoid dismissing any potentially real inhibitors (Supporting Information Figure S5). However, these compounds should only be considered hits if their inhibitory effects could be confirmed from pure powder. We believe it is of utmost importance to share the discovery of all these reproducible screening hits in a timely manner to allow chemistry labs to engage and speed up the discovery of more potent nsp13 inhibitors.

CONCLUSIONS

Since the start of the COVID-19 pandemic, several effective vaccines have been developed and administered worldwide. However, the limited global access to the vaccines combined with emerging new variants and vaccine hesitancy, have made the development of antiviral therapeutics an equally important task in treatment of COVID-19 and prevention of other potentially emerging pandemics. Thus, several antiviral small-molecule drugs have been developed targeting SARS-CoV-2.[32,33] PF-07321332 developed by Pfizer was the main SARS-CoV-2 protease (M^{pro}) inhibitor with in vitro pan-human CoV antiviral activity and orally bioavailable.[32] Pfizer's PAXLOVID received emergency use authorization in December 2021 in the United States.[34] EIDD-2801 was another orally bioavailable prodrug reported.[33] Among all CoV proteins, nsp13 helicase is one of the most important targets for antiviral development given its high conservation and druggability.[10,14,21] Several inhibitors against nsp13 from various CoVs have been identified using various approaches.[22,24,35] These include SSYA10-001, which was identified by screening using a FRET-based helicase assay that specifically prevents the double-stranded (ds)RNA and dsDNA unwinding activities of SARS-CoV nsp13 with IC_{50} values of about 5 μM.[24] Most recently, Gileadi and colleagues identified 65 fragment hits by the crystallographic fragment screening of SARS-CoV-2 nsp13.[12] Such fragments will have to go through extensive chemical optimization to reach a significant inhibitory effect. To further advance the research on discovery of nsp13 inhibitors, we have developed and validated an nsp13 ATPase assay in the presence and absence of ssDNA for high-throughput screening. Given the robustness and cost-effectiveness of these assays, they could easily be employed as a primary assay for screening a large number of small molecules, or as a secondary assay for hit confirmation for other screening options. Particularly, it is invaluable for assessment of a myriad of computationally identified potential inhibitors of nsp13 from various CoVs.[36] Importantly, the discovery of the druglike small-molecule inhibitors of nsp13 we reported here will enable parallel projects by scientific communities that will accelerate discovery of potent and selective inhibitors of CoV replication and propagation.

https://doi.org/10.1021/acsinfecdis.2c00165
ACS Infect. Dis. 2022, 8, 1533−1542

METHODS

Protein Expression and Purification. The expression and purification of SARS-CoV-2 nsp13 are provided in the Supporting Information.

Bioluminescence Assay Developments. The ssDNA$^+$ and ssDNA$^-$ ATPase activities of SARS-CoV-2 nsp13 were monitored in vitro by a bioluminescent assay. In this approach, the level of consumed ATP by the nsp13 enzyme is quantified by measuring the amount of remaining ATP using a luciferase-based assay. We used Kinase-Glo reagents (Cat# V6712; Promega, Madison, WI, USA) for this purpose, which relies on a recombinant thermostable luciferase to generate a luminescent signal (Supporting Information Figure S1). The level of produced bioluminescent signal [measured in relative light units (RLU)] correlates directly with the amount of ATP remaining in each reaction and correlates inversely with the degree of nsp13 ATPase activity. For all the experiments, ATP was used as a substrate in ssDNA$^-$ ATPase reactions, whereas ATP and a 30b PolyT ssDNA were used as substrates for ssDNA$^+$ ATPase activity. All the assay development reactions, unless stated otherwise, were performed in 14 μL volume in 384-well polypropylene microplates (Cat# 784201, Greiner Bio-One) at room temperature (23 °C) in triplicates. For assay optimization, the effects of various additive reagents were investigated individually through titration of the reaction mixture with varying concentrations of NaCl (4−125 mM), KCl (5−150 mM), bovine serum albumin (BSA, 0.002−0.05%), Triton X-100 (0.002−0.05%), DTT (1−50 mM), and DMSO (0.1−5.0%) and evaluating their relative activity compared to the reactions without additive. After completion of the enzymatic reactions, 10 μL of each reaction was transferred into white 384-well plates (Cat# 781207; Greiner) which already contained 10 μL of luciferase reagent per well. Plates were further incubated for 15−20 min at room temperature to allow the bioluminescence signal to develop. The amount of consumed ATP substrate was then quantified by measuring the generated signals using a BioTek Synergy 4 plate reader instrument, and the data were analyzed using MS Excel and GraphPad Prism 9.

Kinetic Characterizations. The kinetic characterization studies of the SARS-CoV-2 nsp13 sDNA$^+$ and ssDNA$^-$ ATPase activities were performed in triplicates at room temperature in the optimized buffer containing 50 mM HEPES, pH = 7.5, 5% glycerol, 5 mM magnesium acetate, 5 mM DTT, and 0.01% BSA in a 384-well plate format and employing the same luciferase reagent for signal detection. The kinetic parameters (K_m and k_{cat}) for the ssDNA$^-$ ATPase were determined using a set of reactions with varying concentrations of ATP substrate (from 0.004 to 6.0 μM). For determining the kinetic parameters of nsp13 ssDNA$^+$ ATPase activity, two sets of experiments were performed for obtaining the K_m values of each substrate. In these tests, the concentration of the one substrate was kept constant at near saturation (>3.0× K_m; 8.5 μM ATP or 12 nM ssDNA), whereas the concentration for the second substrate was varied (0.0003−500 nM ssDNA or 0.004−6 μM ATP). For obtaining endpoint kinetic data, we decided to perform all the reactions simultaneously and to measure the luminescence signals from all the samples in each data set (including ATP standards) at the same time. Therefore, the following approach was devised. Briefly, 140 μL reactions were set up in a 384-well deep-well plate. Experiments were started simultaneously by addition of 0.5 and 0.04 nM nsp13 to ssDNA$^-$ and sDNA$^+$ reactions, respectively, using the 384-well liquid-handling instrument. At different time points (0, 10, 20, 35, 65, 120, and 150 min), 15 μL samples were transferred into Axygen 384-well PCR plates. After the reaction was stopped immediately by heating at 95 °C for 4 min using a 384-well thermocycler (Roche), plates were placed on ice. ATP standard solutions prepared at different concentrations in reaction buffer were also subjected to the same heating process. After heat treatment of the last time-point samples (150 min), all reactions were thermally equilibrated (10 min at room temperature). Then, 12 μL of these solutions were transferred into a white 384-well plate that already contained 12 μL of luciferase reagent per well. The reaction plate was incubated for another 30 min at room temperature following a short spin. The generated luminescence signals were measured using the BioTek Synergy 4 (Vermont, USA) instrument. The initial velocities were calculated from the linear portions of the reaction progression curves, and kinetic parameters were determined using the Michaelis−Menten equation using GraphPad Prism 9 (La Jolla, CA).

Linearity and Z'-Factor Determination. For monitoring the linearity of nsp13 reaction progression over time, time-point experiments were performed in quadruplicates using a buffer containing 50 mM HEPES, pH = 7.5, 5% glycerol, 5 mM magnesium acetate, 5 mM DTT, and 0.01% BSA and the final screening concentrations of substrate(s) and the nsp13 enzyme (i.e., 0.25 μM ATP and 0.1 nM nsp13 for ssDNA$^-$ ATPase and 2.5 μM ATP, 3.5 nM ssDNA, and 0.1 nM nsp13 for the ssDNA$^+$ ATPase). Samples without nsp13 were used as controls for ssDNA$^-$ activity, whereas for the ssDNA$^+$ activity, samples without either nsp13 or ssDNA were used for control. Reactions were started by addition of substrate(s). Samples were taken at different time points (0, 10, 25, 40, 60, and 90 min) and stopped immediately by heating at 95 °C for 3 min (as above). The level of the generated signal in these samples was measured using the luciferase reagent.

The standard Z'-factor determination procedure was used for assessing the quality and robustness of the nsp13 assays. For determining the Z'-factor of ssDNA$^-$, the reaction mixtures containing 0.25 μM ATP substrate in 50 mM HEPES, pH = 7.5, 5% glycerol, 5 mM magnesium acetate, 5 mM DTT, 1.0% DMSO, and 0.01% BSA were set up in the 384-well format in the presence or absence of 0.1 nM nsp13. Reactions were initiated by addition of ATP and were incubated for 60 min at room temperature. After measuring the signal generated by the bioluminescent method, a Z'-factor value was calculated as described previously.[28] For calculating the Z'-factor for the nsp13 ssDNA$^+$, the reaction mixtures (50 mM HEPES, pH = 7.5, 5% glycerol, 5 mM magnesium acetate, 5 mM DTT, 1.0% DMSO, and 0.01% BSA) containing 2.5 μM ATP and 3.5 nM ssDNA were set up in the 384-well format. Reactions were initiated by addition of 0.1 nM of nsp13 and were incubated for 60 min at 23 °C. Reactions lacking either nsp13 or ssDNA were used as controls. The final DMSO concentration was 1%. After measuring the signal generated by the bioluminescent approach, the Z'-factor value was calculated as described above.

Screening a Library of 5000 Small Molecules. SARS-CoV-2 nsp13 was screened against a library of potential kinase inhibitors containing 5000 small molecules (ChemDiv Kinase Library) at 50 μM using the optimized ssDNA$^+$ ATPase assay. The inhibitory effects of compounds were assessed in the 384-

https://doi.org/10.1021/acsinfecdis.2c00165
ACS Infect. Dis. 2022, 8, 1533−1542

well format (14 μL final volume) using reactions composed of 50 mM HEPES, pH = 7.5, 5% glycerol, 5 mM magnesium acetate, 5 mM DTT, and 0.01% BSA, 2.5 μM ATP, 3.5 nM ssDNA, and 0.1 nM of nsp13. Samples containing DMSO only (no compounds) were used as the control. Reactions were started by addition of substrates and incubated for 1 h at room temperature. Then, 10 μL of the reactions were transferred into the white 384-well plates containing 10 μL luciferase reagent and incubated for another 20 min at room temperature. Compounds showing more than 50% inhibition were selected for further analysis. These compounds were then tested in dose-response experiments using the same bioluminescence assay principle but optimized for testing an aminoacyl-tRNA synthetase (counter screen). All counter screen experiments were performed using 0.4 mg/mL yeast tRNA, 40 μM amino acid, 0.3 μM ATP, 50 mM Tris (pH = 7.5), 50 mM KCl, 20 mM $MgCl_2$, 0.1 mg/mL BSA, 1 mM DTT, 0.2 mM spermine, 0.05% NP-40, and 0.15 U/mL inorganic pyrophosphatase. Compounds that did not interfere with the generated signal in this assay were selected as confirmed screening hits and were further assessed for determining their IC_{50} values in $ssDNA^-$ and $ssDNA^+$ ATPase activities.

IC_{50} Determination. For IC_{50} determination tests, compounds were assessed in a set of dose-response experiments against SARS-CoV-2 nsp13 $ssDNA^-$ and $ssDNA^+$ ATPase activities in triplicates. Compounds were first serially diluted in DMSO and were added to the reactions at final concentrations ranging from 195 nM to 400 μM with a final DMSO concentration of 2.0%. The final reaction mixtures consisted of 50 mM HEPES, pH = 7.5, 5% glycerol, 5 mM magnesium acetate, 5 mM DTT, 0.01% BSA, 0.1 nM nsp13, and the optimal concentration of substrates (i.e., 0.25 μM ATP for $ssDNA^-$ and 2.5 μM ATP and 3.5 nM ssDNA for $ssDNA^+$). The reactions were started by addition of substrates and incubated for 1 h at room temperature. The level of enzyme activity was then measured using the luciferase reagent as described above. For both $ssDNA^-$ and $ssDNA^+$ activities, samples containing all the reaction components and DMSO to a final concentration of 2.0% in the presence and absence of the enzyme were used as controls for the 100 and 0% activities, respectively. IC_{50} curves were then generated in GraphPad Prism 9 using the four-parameter logistic equation and variable Hill slope.

Limitations of the Assays. Like any other enzymatic assays, these assays are time-sensitive. The assays should be run long enough until a reliable signal-to-noise ratio is attained. Too long reaction times should also be avoided as reactions may no longer be linear and the inhibitory effect of the compounds may be masked. Importantly, because luciferase is used as a coupling enzyme here, it is important to run a counter screen assay with a distant ATPase protein to filter out any possible false positives that may interfere with the assay signal rather than specific binding.

■ ASSOCIATED CONTENT

Supporting Information

The Supporting Information is available free of charge at https://pubs.acs.org/doi/10.1021/acsinfecdis.2c00165.

Protein expression and purification details, ChemDiv catalogue numbers for selected eight reproducible hits, detection of nsp13 ATPase activities using the bioluminescence assays, SARS-CoV-2 nsp13 purification, assay optimization, tests of the top eight hits in a counter screen, and dose-response analysis of six hits from the original in-house samples (PDF)

■ AUTHOR INFORMATION

Corresponding Author

Masoud Vedadi − *Structural Genomics Consortium, University of Toronto, Toronto, Ontario M5G 1L7, Canada; Department of Pharmacology and Toxicology, University of Toronto, Toronto, Ontario M5S 1A8, Canada;* orcid.org/0000-0002-0574-0169; Phone: 416-432-1980; Email: m.vedadi@utoronto.ca

Authors

Aliakbar Khalili Yazdi − *Structural Genomics Consortium, University of Toronto, Toronto, Ontario M5G 1L7, Canada*

Paknoosh Pakarian − *Structural Genomics Consortium, University of Toronto, Toronto, Ontario M5G 1L7, Canada*

Sumera Perveen − *Structural Genomics Consortium, University of Toronto, Toronto, Ontario M5G 1L7, Canada*

Taraneh Hajian − *Structural Genomics Consortium, University of Toronto, Toronto, Ontario M5G 1L7, Canada*

Vijayaratnam Santhakumar − *Structural Genomics Consortium, University of Toronto, Toronto, Ontario M5G 1L7, Canada;* orcid.org/0000-0002-7001-557X

Albina Bolotokova − *Structural Genomics Consortium, University of Toronto, Toronto, Ontario M5G 1L7, Canada*

Fengling Li − *Structural Genomics Consortium, University of Toronto, Toronto, Ontario M5G 1L7, Canada*

Complete contact information is available at: https://pubs.acs.org/10.1021/acsinfecdis.2c00165

Author Contributions

Experimental design, data analysis and review: A.K.Y. and M.V.; biochemical experiments: A.K.Y.; protein purification: P.P. and T.H.; chemical evaluation of hits: V.S.; assay reproducibility tests: S.P.; review data: F.L.; compound management: A.B.; manuscript writing: A.K.Y. and M.V.; and conceptualization and team supervision: M.V. All authors have reviewed and approved the final version of the manuscript.

Notes

The authors declare no competing financial interest.

■ ACKNOWLEDGMENTS

We would like to thank Ashley Hutchinson, Almagul Seitova, and Peter Loppnau for technical support, and Madhushika Silva for critical review of the manuscript. This research was funded by the University of Toronto COVID-19 Action Initiative-2020 and COVID-19 Mitacs Accelerate postdoctoral award to A.K.Y. and S.P. Structural Genomics Consortium is a registered charity (no: 1097737) that receives funds from Bayer AG, Boehringer Ingelheim, Bristol Myers Squibb, Genentech, Genome Canada through Ontario Genomics Institute [OGI-196], EU/EFPIA/OICR/McGill/KTH/Diamond Innovative Medicines Initiative 2 Joint Undertaking [EUbOPEN grant 875510], Janssen, Merck KGaA (aka EMD in Canada and US), Pfizer, and Takeda.

■ ABBREVIATIONS

SARS-CoV-2, severe acute respiratory syndrome-coronavirus-2; COVID-19, coronavirus disease-2019; NTP, nucleoside

triphosphate; NTPase, nucleoside triphosphatase activity; ssDNA, single-stranded DNA; ZBD, zinc-binding domain; RTC, replication−transcription complex; CoV, coronavirus; RdRp, RNA-dependent RNA polymerase; RTPase, RNA 5′-triphosphatase

REFERENCES

(1) Gorbalenya, A. E.; Baker, S. C.; Baric, R. S.; de Groot, R. J.; Drosten, C.; Gulyaeva, A. A.; Haagmans, B. L.; Lauber, C.; Leontovich, A. M.; Neuman, B. W. The species Severe acute respiratory syndrome-related coronavirus: classifying 2019-nCoV and naming it SARS-CoV-2. *Nat. Microbiol.* **2020**, *5*, 536−544.

(2) Li, G.; Fan, Y.; Lai, Y.; Han, T.; Li, Z.; Zhou, P.; Pan, P.; Wang, W.; Hu, D.; Liu, X.; Zhang, Q.; Wu, J. Coronavirus infections and immune responses. *J. Med. Virol.* **2020**, *92*, 424−432.

(3) Ziebuhr, J. The coronavirus replicase. *Curr. Top. Microbiol. Immunol.* **2005**, *287*, 57−94. V'kovski, P.; Kratzel, A.; Steiner, S.; Stalder, H.; Thiel, V. Coronavirus biology and replication: implications for SARS-CoV-2. *Nat. Rev. Microbiol.* **2021**, *19*, 155−170.

(4) Seybert, A.; Hegyi, A.; Siddell, S. G.; Ziebuhr, J. The human coronavirus 229E superfamily 1 helicase has RNA and DNA duplex-unwinding activities with 5′-to-3′ polarity. *RNA* **2000**, *6*, 1056−1068.

(5) Ivanov, K. A.; Ziebuhr, J. Human Coronavirus 229E Nonstructural Protein 13: Characterization of Duplex-Unwinding, Nucleoside Triphosphatase, and RNA 5′-Triphosphatase Activities. *J. Virol.* **2004**, *78*, 7833−7838.

(6) Ivanov, K. A.; Thiel, V.; Dobbe, J. C.; van der Meer, Y.; Snijder, E. J.; Ziebuhr, J. Multiple enzymatic activities associated with severe acute respiratory syndrome coronavirus helicase. *J. Virol.* **2004**, *78*, 5619−5632.

(7) Tanner, J. A.; Watt, R. M.; Chai, Y.-B.; Lu, L.-Y.; Lin, M. C.; Peiris, J. S. M.; Poon, L. L. M.; Kung, H.-F.; Huang, J.-D. The Severe Acute Respiratory Syndrome (SARS) Coronavirus NTPase/Helicase Belongs to a Distinct Class of 5′ to 3′ Viral Helicases. *J. Biol. Chem.* **2003**, *278*, 39578−39582.

(8) Lehmann, K. C.; Snijder, E. J.; Posthuma, C. C.; Gorbalenya, A. E. What we know but do not understand about nidovirus helicases. *Virus Res.* **2015**, *202*, 12−32.

(9) Zhang, R.; Li, Y.; Cowley, T. J.; Steinbrenner, A. D.; Phillips, J. M.; Yount, B. L.; Baric, R. S.; Weiss, S. R. The nsp1, nsp13, and M proteins contribute to the hepatotropism of murine coronavirus JHM.WU. *J. Virol.* **2015**, *89*, 3598−3609.

(10) Chen, J.; Malone, B.; Llewellyn, E.; Grasso, M.; Shelton, P. M. M.; Olinares, P. D. B.; Maruthi, K.; Eng, E. T.; Vatandaslar, H.; Chait, B. T.; Kapoor, T. M.; Darst, S. A.; Campbell, E. A. Structural Basis for Helicase-Polymerase Coupling in the SARS-CoV-2 Replication-Transcription Complex. *Cell* **2020**, *182*, 1560−1573.

(11) Nga, P. T.; Parquet, M. C.; Lauber, C.; Parida, M.; Nabeshima, T.; Yu, F.; Thuy, N. T.; Inoue, S.; Ito, T.; Okamoto, K.; Ichinose, A.; Snijder, E. J.; Morita, K.; Gorbalenya, A. E. Discovery of the first insect nidovirus, a missing evolutionary link in the emergence of the largest RNA virus genomes. *PLoS Pathog.* **2011**, *7*, No. e1002215.

(12) Newman, J. A.; Douangamath, A.; Yadzani, S.; Yosaatmadja, Y.; Aimon, A.; Brandão-Neto, J.; Dunnett, L.; Gorrie-Stone, T.; Skyner, R.; Fearon, D.; Schapira, M.; von Delft, F.; Gileadi, O. Structure, mechanism and crystallographic fragment screening of the SARS-CoV-2 NSP13 helicase. *Nat. Commun.* **2021**, *12*, 4848.

(13) Hao, W.; Wojdyla, J. A.; Zhao, R.; Han, R.; Das, R.; Zlatev, I.; Manoharan, M.; Wang, M.; Cui, S. Crystal structure of Middle East respiratory syndrome coronavirus helicase. *PLoS Pathog.* **2017**, *13*, No. e1006474.

(14) Jia, Z.; Yan, L.; Ren, Z.; Wu, L.; Wang, J.; Guo, J.; Zheng, L.; Ming, Z.; Zhang, L.; Lou, Z.; Rao, Z. Delicate structural coordination of the Severe Acute Respiratory Syndrome coronavirus Nsp13 upon ATP hydrolysis. *Nucleic Acids Res.* **2019**, *47*, 6538−6550.

(15) Yan, L.; Ge, J.; Zheng, L.; Zhang, Y.; Gao, Y.; Wang, T.; Huang, Y.; Yang, Y.; Gao, S.; Li, M.; Liu, Z.; Wang, H.; Li, Y.; Chen, Y.; Guddat, L. W.; Wang, Q.; Rao, Z.; Lou, Z. Cryo-EM Structure of an Extended SARS-CoV-2 Replication and Transcription Complex Reveals an Intermediate State in Cap Synthesis. *Cell* **2021**, *184*, 184−193.

(16) Jankowsky, E.; Fairman, M. E. RNA helicases - one fold for many functions. *Curr. Opin. Struct. Biol.* **2007**, *17*, 316−324.

(17) Snijder, E. J.; Decroly, E.; Ziebuhr, J. The Nonstructural Proteins Directing Coronavirus RNA Synthesis and Processing. *Adv. Virus Res.* **2016**, *96*, 59−126.

(18) Walker, J. E.; Saraste, M.; Runswick, M. J.; Gay, N. J. Distantly related sequences in the alpha- and beta-subunits of ATP synthase, myosin, kinases and other ATP-requiring enzymes and a common nucleotide binding fold. *EMBO J.* **1982**, *1*, 945−951.

(19) Adedeji, A. O.; Singh, K.; Sarafianos, S. G. Structural and biochemical basis for the difference in the helicase activity of two different constructs of SARS-CoV helicase. *Cell. Mol. Biol.* **2012**, *58*, 114−121.

(20) Devarkar, S. C.; Wang, C.; Miller, M. T.; Ramanathan, A.; Jiang, F.; Khan, A. G.; Patel, S. S.; Marcotrigiano, J. Structural basis for m7G recognition and 2′-O-methyl discrimination in capped RNAs by the innate immune receptor RIG-I. *Natl. Acad. Sci. U.S.A.* **2016**, *113*, 596−601.

(21) Yazdani, S.; De Maio, N.; Ding, Y.; Shahani, V.; Goldman, N.; Schapira, M. Genetic Variability of the SARS-CoV-2 Pocketome. *J. Proteome Res.* **2021**, *20*, 4212−4215.

(22) Shadrick, W. R.; Ndjomou, J.; Kolli, R.; Mukherjee, S.; Hanson, A. M.; Frick, D. N. Discovering new medicines targeting helicases: challenges and recent progress. *J. Biomol. Screen* **2013**, *18*, 761−781. Yu, M.-S.; Lee, J.; Lee, J. M.; Kim, Y.; Chin, Y.-W.; Jee, J.-G.; Keum, Y.-S.; Jeong, Y.-J. Identification of myricetin and scutellarein as novel chemical inhibitors of the SARS coronavirus helicase, nsP13. *Bioorg. Med. Chem. Lett.* **2012**, *22*, 4049−4054.

(23) Keum, Y.-S.; Jeong, Y.-J. Development of chemical inhibitors of the SARS coronavirus: viral helicase as a potential target. *Biochem. Pharmacol.* **2012**, *84*, 1351−1358. Yan, L.; Zhang, Y.; Ge, J.; Zheng, L.; Gao, Y.; Wang, T.; Jia, Z.; Wang, H.; Huang, Y.; Li, M.; Wang, Q.; Rao, Z.; Lou, Z. Architecture of a SARS-CoV-2 mini replication and transcription complex. *Nat. Commun.* **2020**, *11*, 5874.

(24) Adedeji, A. O.; Singh, K.; Calcaterra, N. E.; DeDiego, M. L.; Enjuanes, L.; Weiss, S.; Sarafianos, S. G. Severe acute respiratory syndrome coronavirus replication inhibitor that interferes with the nucleic acid unwinding of the viral helicase. *Antimicrob. Agents Chemother.* **2012**, *56*, 4718−4728.

(25) Adedeji, A. O.; Lazarus, H. Biochemical Characterization of Middle East Respiratory Syndrome Coronavirus Helicase. *mSphere* **2016**, *1*, No. e00235.

(26) Eickhoff, P.; Kose, H. B.; Martino, F.; Petojevic, T.; Abid Ali, F.; Locke, J.; Tamberg, N.; Nans, A.; Berger, J. M.; Botchan, M. R.; Yardimci, H.; Costa, A. Molecular Basis for ATP-Hydrolysis-Driven DNA Translocation by the CMG Helicase of the Eukaryotic Replisome. *Cell Rep.* **2019**, *28*, 2673−2688.

(27) Iversen, P. W.; Eastwood, B. J.; Sittampalam, G. S.; Cox, K. L. A Comparison of Assay Performance Measures in Screening Assays: Signal Window, Z′ Factor, and Assay Variability Ratio. *J. Biomol. Screen* **2006**, *11*, 247−252.

(28) Zhang, J.-H.; Chung, T. D. Y.; Oldenburg, K. R. A Simple Statistical Parameter for Use in Evaluation and Validation of High Throughput Screening Assays. *J. Biomol. Screen* **1999**, *4*, 67−73.

(29) Shoichet, B. K. Interpreting steep dose-response curves in early inhibitor discovery. *J. Med. Chem.* **2006**, *49*, 7274−7277. Chen, X.; Ali, Y. I.; Fisher, C. E.; Arribas-Bosacoma, R.; Rajasekaran, M. B.; Williams, G.; Walker, S.; Booth, J. R.; Hudson, J. J.; Roe, S. M.; Pearl, L. H.; Ward, S. E.; Pearl, F. M.; Oliver, A. W. Uncovering an allosteric mode of action for a selective inhibitor of human Bloom syndrome protein. *Elife* **2021**, *10*, No. e65339.

(30) O'Donnell, H. R.; Tummino, T. A.; Bardine, C.; Craik, C. S.; Shoichet, B. K. Colloidal Aggregators in Biochemical SARS-CoV-2 Repurposing Screens. *J. Med. Chem.* **2021**, *64*, 17530−17539.

https://doi.org/10.1021/acsinfecdis.2c00165
ACS Infect. Dis. 2022, 8, 1533−1542

(31) Torosyan, H.; Shoichet, B. K. Protein Stability Effects in Aggregate-Based Enzyme Inhibition. *J. Med. Chem.* **2019**, *62*, 9593−9599.
(32) Owen, D. R.; Allerton, C. M. N.; Anderson, A. S.; Aschenbrenner, L.; Avery, M.; Berritt, S.; Boras, B.; Cardin, R. D.; Carlo, A.; Coffman, K. J.; Dantonio, A.; Di, L.; Eng, H.; Ferre, R.; Gajiwala, K. S.; Gibson, S. A.; Greasley, S. E.; Hurst, B. L.; Kadar, E. P.; Kalgutkar, A. S.; Lee, J. C.; Lee, J.; Liu, W.; Mason, S. W.; Noell, S.; Novak, J. J.; Obach, R. S.; Ogilvie, K.; Patel, N. C.; Pettersson, M.; Rai, D. K.; Reese, M. R.; Sammons, M. F.; Sathish, J. G.; Singh, R. S. P.; Steppan, C. M.; Stewart, A. E.; Tuttle, J. B.; Updyke, L.; Verhoest, P. R.; Wei, L.; Yang, Q.; Zhu, Y. An oral SARS-CoV-2 M pro inhibitor clinical candidate for the treatment of COVID-19. *Science* **2021**, *374*, 1586−1593.
(33) Wahl, A.; Gralinski, L. E.; Johnson, C. E.; Yao, W.; Kovarova, M.; Dinnon, K. H., 3rd; Liu, H.; Madden, V. J.; Krzystek, H. M.; De, C.; White, K. K.; Gully, K.; Schäfer, A.; Zaman, T.; Leist, S. R.; Grant, P. O.; Bluemling, G. R.; Kolykhalov, A. A.; Natchus, M. G.; Askin, F. B.; Painter, G.; Browne, E. P.; Jones, C. D.; Pickles, R. J.; Baric, R. S.; Garcia, J. V. SARS-CoV-2 infection is effectively treated and prevented by EIDD-2801. *Nature* **2021**, *591*, 451−457.
(34) Lamb, Y. N. Nirmatrelvir Plus Ritonavir: First Approval. *Drugs* **2022**, *82*, 585.
(35) Lee, C.; Lee, J. M.; Lee, N.-R.; Jin, B.-S.; Jang, K. J.; Kim, D.-E.; Jeong, Y.-J.; Chong, Y. Aryl diketoacids (ADK) selectively inhibit duplex DNA-unwinding activity of SARS coronavirus NTPase/helicase. *Bioorg. Med. Chem. Lett.* **2009**, *19*, 1636−1638. Chen, T.; Fei, C.-Y.; Chen, Y.-P.; Sargsyan, K.; Chang, C.-P.; Yuan, H. S.; Lim, C. Synergistic Inhibition of SARS-CoV-2 Replication Using Disulfiram/Ebselen and Remdesivir. *ACS Pharmacol. Transl. Sci.* **2021**, *4*, 898−907.
(36) Mirza, M. U.; Froeyen, M. Structural elucidation of SARS-CoV-2 vital proteins: Computational methods reveal potential drug candidates against main protease, Nsp12 polymerase and Nsp13 helicase. *J. Pharm. Anal.* **2020**, *10*, 320−328. Naik, B.; Gupta, N.; Ojha, R.; Singh, S.; Prajapati, V. K.; Prusty, D. High throughput virtual screening reveals SARS-CoV-2 multi-target binding natural compounds to lead instant therapy for COVID-19 treatment. *Int. J. Biol. Macromol.* **2020**, *160*, 1−17. White, M. A.; Lin, W.; Cheng, X. Discovery of COVID-19 Inhibitors Targeting the SARS-CoV-2 Nsp13 Helicase. *J. Phys. Chem. Lett.* **2020**, *11*, 9144−9151. Freidel, M. R.; Armen, R. S. Mapping major SARS-CoV-2 drug targets and assessment of druggability using computational fragment screening: Identification of an allosteric small-molecule binding site on the Nsp13 helicase. *PLoS One* **2021**, *16*, No. e0246181. Gorgulla, C.; Padmanabha Das, K. M.; Leigh, K. E.; Cespugli, M.; Fischer, P. D.; Wang, Z.-F.; Tesseyre, G.; Pandita, S.; Shnapir, A.; Calderaio, A.; Gechev, M.; Rose, A.; Lewis, N.; Hutcheson, C.; Yaffe, E.; Luxenburg, R.; Herce, H. D.; Durmaz, V.; Halazonetis, T. D.; Fackeldey, K.; Patten, J. J.; Chuprina, A.; Dziuba, I.; Plekhova, A.; Moroz, Y.; Radchenko, D.; Tarkhanova, O.; Yavnyuk, I.; Gruber, C.; Yust, R.; Payne, D.; Näär, A. M.; Namchuk, M. N.; Davey, R. A.; Wagner, G.; Kinney, J.; Arthanari, H. A multi-pronged approach targeting SARS-CoV-2 proteins using ultra-large virtual screening. *iScience* **2021**, *24*, 102021. El Hassab, M. A.; Eldehna, W. M.; Al-Rashood, S. T.; Alharbi, A.; Eskandrani, R. O.; Alkahtani, H. M.; Elkaeed, E. B.; Abou-Seri, S. M. Multi-stage structure-based virtual screening approach towards identification of potential SARS-CoV-2 NSP13 helicase inhibitors. *J. Enzyme Inhib. Med. Chem.* **2022**, *37*, 563−572. Liu, Y.; Gan, J.; Wang, R.; Yang, X.; Xiao, Z.; Cao, Y. DrugDevCovid19: An Atlas of Anti-COVID-19 Compounds Derived by Computer-Aided Drug Design. *Molecules* **2022**, *27*, 683. Perez-Lemus, G. R.; Menéndez, C. A.; Alvarado, W.; Byléhn, F.; de Pablo, J. J. Toward wide-spectrum antivirals against coronaviruses: Molecular characterization of SARS-CoV-2 NSP13 helicase inhibitors. *Sci. Adv.* **2022**, *8*, No. eabj4526.

https://doi.org/10.1021/acsinfecdis.2c00165
ACS Infect. Dis. 2022, 8, 1533−1542